

# Extended-Time Multitaper Frequency Domain Cross-Correlation Receiver-Function Estimation

by George Helffrich

**Abstract** This article documents a method that successfully yields frequency-domain cross-correlation receiver functions without losing amplitude at long time lags and without sacrificing any of the advantages of the method. After a description of this method, an analysis of synthetics of transition zone structure shows that it provides a way to investigate mantle structure from the surface through the transition zone and deeper.

## Introduction

The receiver-function method is a common analysis technique of great conceptual simplicity and is widely used by seismologists. The method relies on the insight that the coda following a teleseismic body-wave arrival largely consists of mode-converted energy emanating from the impedance contrasts arising from layering in the earth near the receiver (Phinney, 1964). As such, this mode-converted wave train is a convolution of the incident wave with the earth structure. Under the geologically reasonable approximation of horizontal layering (which later extensions to the method relax), deconvolving the vertical component of the *P*-wave arrival (an estimate of the incident wave) from the radial component (the mode-converted wave train) yields an estimate of the earth structure: a sequence of pulses in time produced by the incident wave field, also called the receiver function. The concept is simple, but reliable implementation is difficult.

The implementation difficulties stem from the instability of deconvolution. This led to the use of a variety of stabilization methods to estimate the receiver function. Those methods include frequency-domain division with a spectral water level (Langston, 1979; Owens *et al.*, 1983; Ammon, 1991), deconvolution in the time domain by least-squares estimation (Abers *et al.*, 1995), iterative deconvolution in the time domain (Ligorria and Ammon, 1999), and multitaper frequency-domain cross-correlation receiver function (MTRF) (Park and Levin, 2000). Park and Levin (2000) compare and contrast the methods, to which I refer the reader interested in those issues. One key advantage of the MTRF is its resistance to noise, which recommends its use in environments such as ocean islands with high noise levels in the seismic band. This advantage is due to MTRF's use of multitapers to minimize spectral leakage and its frequency-dependent downweighting of the noisy portions of the spectrum. A disadvantage of the Park and Levin (2000) MTRF method (P&L MTRF, hereafter) is that only the first 10 sec or so of the receiver function contain a usable signal. The

receiver-function amplitude decays at longer lags, principally because of the short analysis windows (about 60 sec, but extendable for some target time-bandwidth products) forced by the assumption inherent in the use of multiple tapers that the signal is stationary through the taper duration (Thomson, 1982; Park *et al.*, 1987; Park and Levin, 2000, 2005). This defeats the direct use of MTRF for transition zone structure studies, but there are remedies if one is willing to sacrifice continuity of the receiver function from zero to long lags (Park and Levin, 2005). Continuity, however, is a crucial factor if one wishes to migrate a collection of receiver functions in a common conversion point gather to form vertical structure sections through the crust and mantle, as, for example, in Dueker and Sheehan (1997).

This combination of attractive properties and drawbacks motivated a development effort to compute MTRFs in a way that preserves their amplitudes for arbitrarily long times. The description follows in the next paragraphs, plus, with deconvolved synthetics for transition zone structure, a demonstration of the method's ability to surmount the amplitude decay problem at long lags.

## Method

The method is akin to an overlap-and-sum technique for estimating stationary signal spectra in long time series (Press *et al.*, 1992). Unlike overlap-and-sum spectral estimation, however, it preserves phase information by using a sequence of short multiple tapers to window the time series over its full length and to sum the individual Fourier transformed (FT) signals into a frequency-domain representation that preserves the phase lags for each subwindow of the time series. These ideas are sketched in Figure 1.

In practice, for data sampled at 20 Hz, three  $2.5\pi$  prolate tapers of 10-sec duration for windowing, with 50% window overlap work well. Each taper windows the data in the whole-analysis segment after which the FT is calculated and

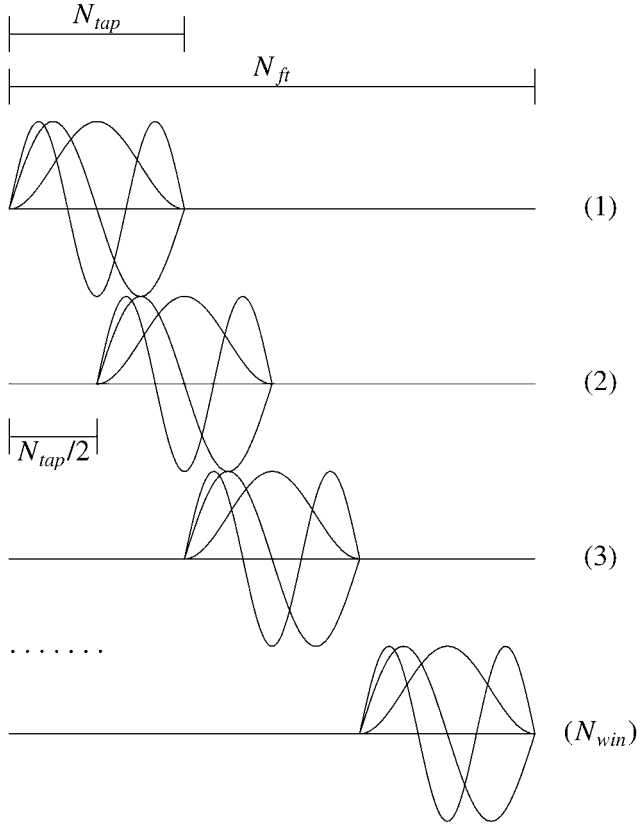


Figure 1. Sketch of construction method for  $K = 3$  Slepian tapers. The duration of the analysis segment is given by the  $N_{ft}$  points indicated by the top bar. The multiple tapers select each windowing interval of  $N_{tap}$  points, and a full  $N_{ft}$  point FT is taken of the whole-analysis segment and accumulated  $N_{win}$  times for each tapered trace FT  $Y^{(k)}(f)$ ,  $k = 1, \dots, K$ . The  $K$  individual taper spectra are combined in the standard way for leakage resistance.

summed with previous FTs for that taper. After that, the standard methods for forming multitaper spectral estimates (Thomson, 1982; Park *et al.*, 1987) lead to a receiver-function estimate  $H_R(f)$  by calculating the cross-correlation of the radial ( $R$ ) component with the vertical ( $Z$ ) component Fourier transform, with use of the prearrival  $Z$ -component power as an estimate of the noise at a particular frequency for weighting (see also Park and Levin [2000]):

$$H_R(f) = \frac{\sum_{k=1}^K (Y_Z^{(k)}(f))^* Y_R^{(k)}(f)}{S_0(f) + \sum_{k=1}^K (Y_Z^{(k)}(f))^* Y_Z^{(k)}(f)}. \quad (1)$$

Here  $Y_{R,Z}^{(k)}$  are the  $k$ th of  $K$  Slepian-tapered FTs of the  $R$ - or  $Z$ -component signal,  $S_0(f)$  is the spectrum estimate of the pre-event noise on the vertical component, and  $*$  represents complex conjugation. Applying a  $\cos^2$  frequency-domain taper implements a high-frequency cutoff to the receiver function. Along with the multiple windows, this leads to normalization factors for the spectra that read,

$$\frac{1}{N_{win}} \times \frac{N_{ft}}{N_{fc}} \times \frac{2}{N_{ft}}, \quad (2)$$

multiwindow       $\cos^2$  window      FFT normalization

where  $N_{win}$  is the number of windows contributing to the sum,  $N_{ft}$  is the number of points in the FT, and  $N_{fc}$  is the number of nonzero points in the  $\cos^2$  taper. Because the overlap is the same in every  $Y_{R,Z}^{(k)}$ , no explicit correction is needed for it. The result is a receiver function as long as the original analysis segment. A useful way to distinguish

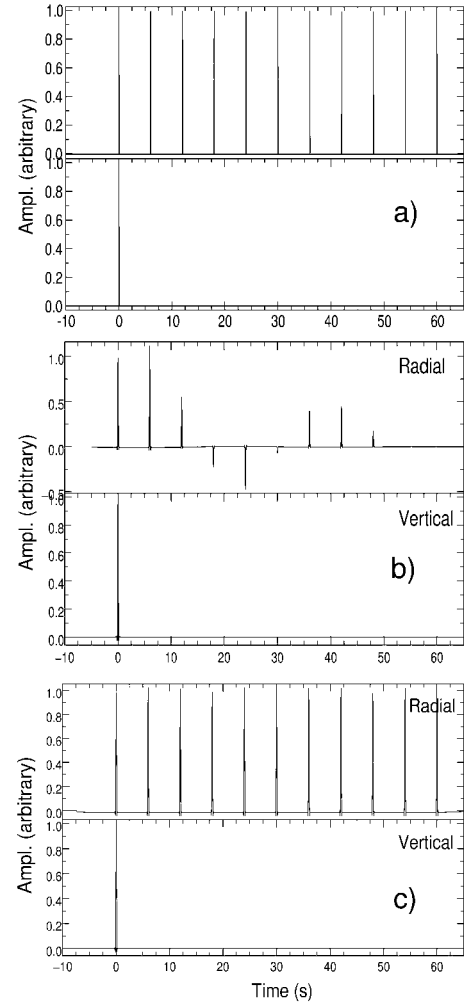


Figure 2. Example of a string of unit impulse functions deconvolved with single unit impulse. The sampling rate is 20 Hz and the deconvolution frequency cutoff is 8 Hz. (a) Synthetic impulse string and single unit impulse deconvolved from the impulse string. (b) P&L MTRF deconvolution. The measurement window starts 10 sec before the first impulse and extends to 50 sec after it. (c) ET MTRF deconvolution. The measurement window starts 5 sec before the first impulse and extends to 65 sec after it. Note nonconstancy of amplitude through measurement window in P&L MTRF as compared with approximately constant amplitude  $\pm 2\%$  for ET MTRF.

this from the P&L MTRF would be to call it an extended-time MTRF, or ET MTRF.

### Examples

Figure 2 shows an example in which a single unit impulse is deconvolved from a train of unit impulse functions spaced every 6 sec from zero to 60 sec. Note two items in the example. First, there is uniform amplitude through the

analysis window, as compared with varying amplitude when a single tapering position is used. Second, amplitudes vary mildly by about 2% through the receiver function. Both of these characteristics arise because the tapers are not uniformly sensitive to an impulse in the taper window. Recall that multitapers are designed for spectral estimation of stationary signals (Thomson, 1982; Park *et al.*, 1987); impulse functions are not of this category.

Figure 3 shows a reflectivity synthetic of a *P*-wave ar-

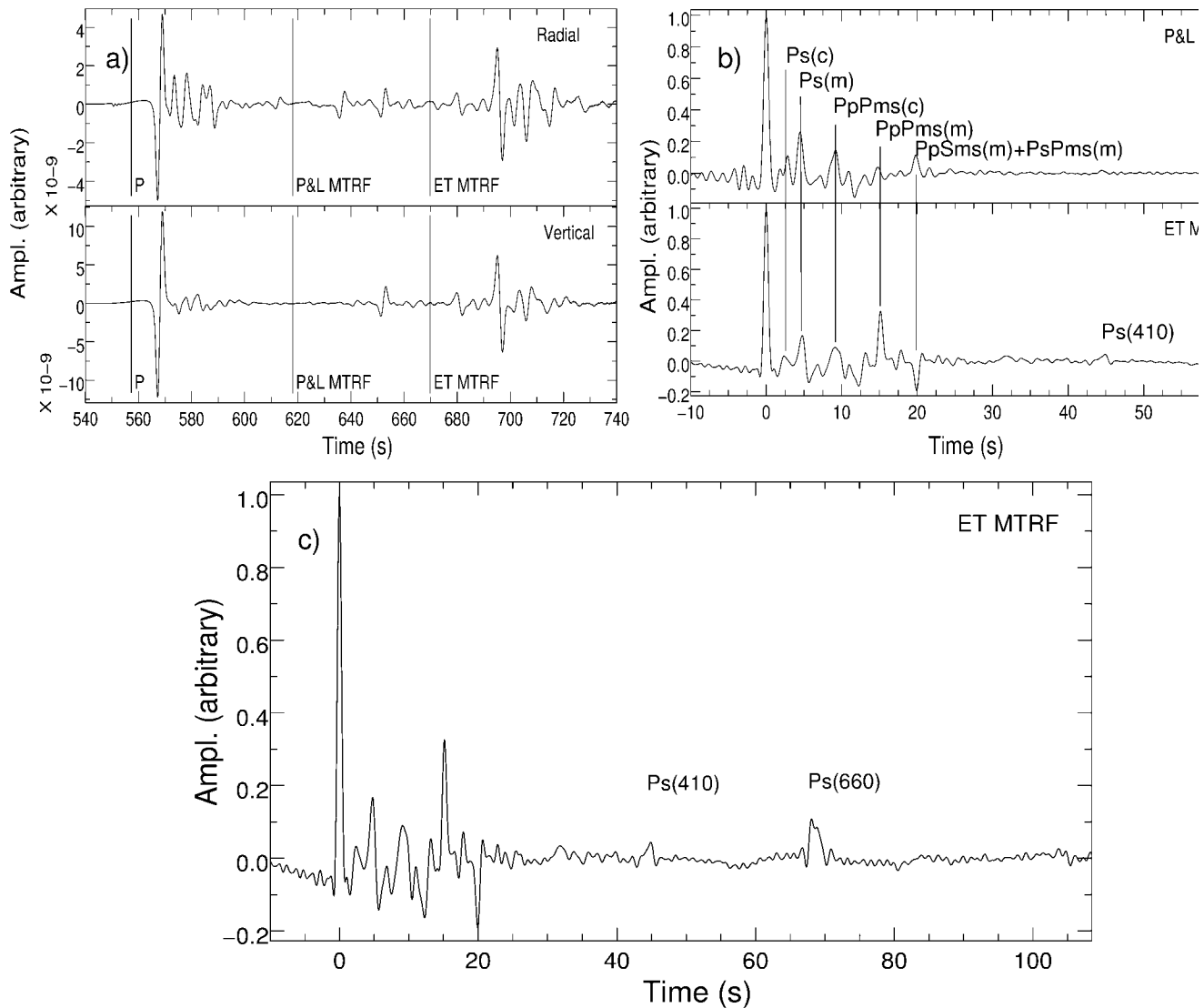


Figure 3. Example of reflectivity velocity seismogram using the SP6 model with source at 60° distance and 400 km depth, deconvolved by using the ET MTRF and P&L MTRF. (a) Top panels indicate radial and vertical synthetic seismograms. Vertical lines mark beginning and end of measurement windows for the P&L and ET MTRFs; both start at the *P* marker. (b) Estimated radial receiver function using the P&L and ET MTRFs. Frequency cutoff is 1.5 Hz. Note that P&L MTRF amplitude drops after 10 sec, whereas the ET MTRF amplitude is sustained to the end of the window. Crustal and mantle *Ps* conversions and reverberations marked (c, intracrustal discontinuity at 20 km; m, Moho at 35 km). (c) ET MTRF for whole measurement interval shown in (a). Note preservation of shallow structure and reverberations between 0 and 20 sec, as well as the prominent arrivals from the 410 and 660 km depth at 44 and 67 sec. Mild undulation is due to low-frequency numerical noise in the synthetic.

rival from a 400-km-deep source located at 60 deg distance from a receiver and the deconvolution of the vertical component from the radial. The reference model is SP6 (Morelli and Dziewonski, 1993), with discontinuities at 20 (intra-crustal), 35 (Moho), 210 (*S* only), 410, and 660 km depth. For comparison, we show the same seismograms deconvolved using Park and Levin's (2000) method with the same analysis window. Agreement in the initial portions of the traces is excellent. The ET MTRF function, in addition, features prominent arrivals from the *P*-to-*S* conversions at 410 and 660 km depth at  $\sim 44$  sec and  $\sim 68$  sec. However, it also contains a complete record of the crustal structure as well, with middle-crust and Moho conversions at  $\sim 2.5$  and  $\sim 4$  sec, and their reverberations.

### Conclusion

The purpose of this article is to introduce the ET MTRF and to demonstrate the viability of using multitaper cross-correlation estimation of receiver functions without requiring short analysis windows. The method described here is capable of being used for receiver-function investigations where estimates at long lags are required, in, for example, transition zone structure investigations.

### Acknowledgments

I thank Jeff Park for a preprint, discussions about the method, and the code to calculate the P&L MTRF.

### References

- Abers, G. A., X. Hu, and L. R. Sykes (1995). Source scaling of earthquakes in the Shumagin region, Alaska: time-domain inversions of regional waveforms, *Geophys. J. Int.* **123**, 41–58.
- Ammon, C. J. (1991). The isolation of receiver effects from teleseismic P waveforms, *Bull. Seism. Soc. Am.* **81**, 2504–2510.
- Dueker, K. D., and A. F. Sheehan (1997). Mantle discontinuity structure from midpoint stacks of converted P to S waves across the Yellowstone hotspot track, *J. Geophys. Res.* **102**, 8313–8327.
- Langston, C. A. (1979). Structure under Mount Rainier, Washington, inferred from teleseismic body waves, *J. Geophys. Res.* **84**, 4749–4762.
- Ligorria, J. P., and C. J. Ammon (1999). Iterative deconvolution and receiver-function estimation, *Bull. Seism. Soc. Am.* **89**, 1395–1400.
- Morelli, A., and A. M. Dziewonski (1993). Body wave traveltimes and a spherically symmetric P- and S-wave velocity model, *Geophys. J. Int.* **112**, 178–194.
- Owens, T. J., S. R. Taylor, and G. Zandt (1983). Isolation and enhancement of the response of local seismic structure from teleseismic P-waveforms, Lawrence Livermore Lab. Report UCID 19809, 1–33.
- Park, J., and V. Levin (2000). Receiver functions from multiple-taper spectral correlation estimates, *Bull. Seism. Soc. Am.* **90**, 1507–1520.
- Park, J., and V. Levin (2005). Receiver functions from multiple-taper spectral correlation: Statistics, single-station migration, and jackknife uncertainty, *Geophys. J. Int.* (in press).
- Park, J., C. R. Lindberg, and F. L. Vernon III (1987). Multitaper analysis of high-frequency seismograms, *J. Geophys. Res.* **92**, 12,675–12,684.
- Phinney, R. A. (1964). Structure of earths crust from spectral behavior of long-period body waves, *J. Geophys. Res.* **69**, 2997–3017.
- Press, W. H., S. A. Teukolsky, W. T. Vetterling, and B. P. Flannery (1992). *Numerical Recipes*, Second Ed., Cambridge University Press, Cambridge, United Kingdom, xxvi + 963 pp.
- Thomson, D. J. (1982). Spectrum estimation and harmonic analysis, *IEEE Proc.* **70**, 1055–1096.

Earth Sciences  
University of Bristol  
Wills Mem. Bldg., Queen's Road  
Bristol BS8 1RJ, United Kingdom

Manuscript received 13 May 2005.